Using Aerial Photos to Produce Digital Surface Models, Orthophotos, and Land Cover Maps of a Coastal Area in Puget Sound, WA

Jonnie Dunne

A thesis submitted in partial fulfillment of the
requirements for the degree of

Master of Science

University of Washington

2015

Committee:
L. Monika Moskal
James Brennan
Miles Logsdon

Program Authorized to Offer Degree:
School of Environmental and Forest Sciences

Abstract

Using aerial photos to produce Digital Surface Models, orthophotos, and land cover maps of a coastal area in Puget Sound, WA.

Jonnie Dunne

Chair of Supervisory Committee:
Dr. L. Monika Moskal
School of Environmental and Forest Science

A new method in photogrammetry (the practice of taking spatial measurements from photographs) called Structure from Motion (SfM) produces automated measurements at much lower cost than older techniques. Research has shown that the spatial resolution and accuracy of measurements taken from SfM varies with photo properties such as camera position (terrestrial, aerial), spectral resolution (black and white, color, near infrared), and subject matter (bare earth, buildings, trees). Our first goal was to assess the spatial resolution and accuracy of SfM measurements taken from color infrared aerial photos of a 400 hectare coastal peninsula. We did so by producing and validating several types of Digital Surface Model (DSM, maps displaying elevation data) and orthophotos (photo maps that have been geometrically corrected using elevation data such that the scale is uniform). Results show that SfM measurements we derived from aerial photos are of high spatial resolution (5 points/m^2) and accuracy. Orthophotos and DSMs derived from similar SfM measurements have been shown to be suitable for many common geospatial applications, but SfM measurements have not yet been used to produce comprehensive land cover maps. Our second goal was to assess the accuracy of a land cover map derived from fusing a DSM and orthophoto and analyzing similarity between adjacent areas using a technique called Object Based Image Analysis. The land cover map we designed is intended to be suitable for monitoring and regulating land cover at small spatial scales in order to evaluate anthropogenic alterations toward conservation of shoreline ecological function. In this case we have semi-automatically mapped trees, shrubs, groundcover vegetation, bare ground, impervious surfaces, and water with 86% accuracy, and much higher resolution than the best available land cover map of the same area. We believe that the low cost of SfM measurements, and the high accuracy and resolution of products derived from them make SfM well suited to aid in monitoring and regulating land use to conserve shoreline ecological function.

Keywords: photogrammetry, Digital Surface Model, orthophoto, Object Based Image Analysis, Land Use Land Cover

Table of Contents

List of Figures

List of Tables

Acknowledgements

This research has been supported by the School of Environmental and Forest Science, Klemme Scholarship, the Precision Forestry Cooperative, and carried out in the University of Washington Remote Sensing and Geospatial Analysis Laboratory (RSGAL).

Thank you to my committee, L. Monika Moskal, PhD (chair), Miles Logsdon, PhD, and James Brennan, MS, for providing me with assistance and advice based on their expertise.

Thank you to the City of Bainbridge Island for access to the aerial photography used in this study, to the King County GIS Center for access to aerial photography metadata, to Agisoft for software support, to the Quaternary Research Lab of the Earth and Space Sciences Dept for access to critical computer hardware and software, and the Precision Forestry Cooperative at the UW for providing administrative assistance.

Many thanks to my colleagues at the RSGAL including Meghan Halabisky, Jeff Richardson, Chris Vondrasek, Caileigh Shoot, and Patrick Mi for helpful support, guidance, and critique. Thank you also to Brendan Dunne for editorial assistance.

Huge thank you to Clarice for strong emotional and moral support, as well as assistance with fieldwork.

1. Introduction

1.1 Background

Recent advances in photogrammetry, the practice of taking spatial measurements from photographs, allow software users to take measurements with greater speed and resolution at lower cost than ever before. These qualities have shown the potential to improve many geospatial applications of photogrammetric measurements such as Digital Surface Model (DSM, Figure 1) and orthophoto (Figure 2) production (Lane et al. 2000, Leberl & Thurgood 2004, Jancso & Melykuti 2011, Fonstad et al. 2013). However, the accuracy and spatial resolution of photogrammetric measurements varies with photo properties such as camera position (terrestrial, aerial), spectral resolution (black and white, color, near infrared), and subject matter (bare earth, buildings, trees), which in turn affects the utility of DSMs and orthophotos derived from the photogrammetry measurements (Dandois & Ellis 2013, Nebiker et al. 2014, Gomez et al. 2015). The purpose of this research was to first study the accuracy and spatial resolution of photogrammetry measurements taken from high spatial resolution (0.15m Ground Sample Distance, GSD) color infrared aerial photos of a coastal area in Puget Sound, WA. We then evaluated the utility of DSMs and orthophotos derived from those photogrammetry measurements for producing a high spatial resolution land cover map. The results of these studies are of particular interest to land managers in Washington State, where high resolution, low cost land cover maps can aid in meeting legal requirements to evaluate and regulate shoreline development in such a way that conserves shoreline ecological function.

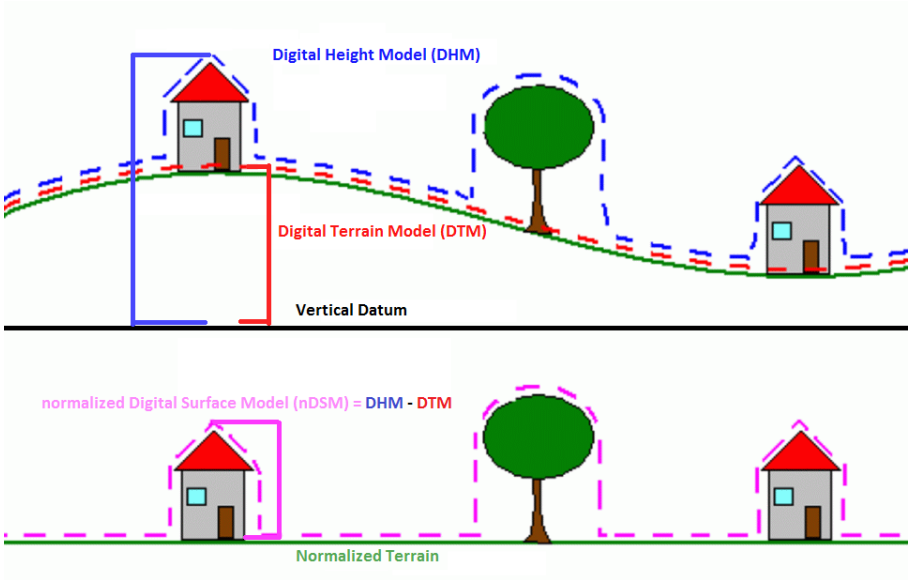

Figure 1. A Digital Surface Model (DSM) consists of georeferenced gridded surface elevation data of various types such as: a Digital Height Model (DHM), which displays the elevation of the upper surface of a landscape above a vertical datum including buildings and treetops; a Digital Terrain Model (DTM), which shows the elevation of only the ground surface above a vertical datum; and a Normalized Digital Surface Model (nDSM), which is produced by subtracting DTM heights from DHM heights to calculate the elevation of objects above the normalized terrain. (Adapted from Mayer 2004)

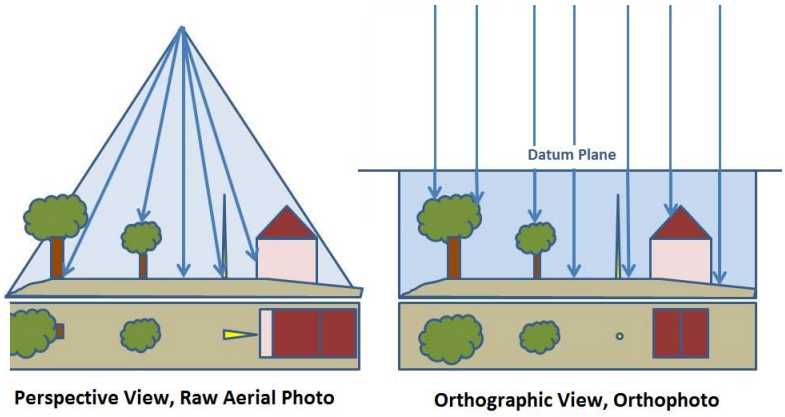

Figure 2. Raw aerial photos provide a perspective view (A) in which the distance between the viewpoint and objects varies, resulting in variable scale and distortion which is unsuitable for geospatial applications. Orthophotos that have been distorted to fit a DSM and projected onto a reference datum plane provide an orthographic view (B), where the distances between objects and viewpoint are effectively infinite which results in uniform scale and eliminates distortion (Adapted from Aerometrex 2013).

The goal of the Washington State Shoreline Management Act is to “prevent the inherent harm in an uncoordinated and piecemeal development of the state’s shorelines" (Crooks 1973). The act requires 39 counties and over 200 towns and cities to develop a Shoreline Master Program (SMP), a localized combined comprehensive plan, zoning ordinance, and permitting system that regulate shoreline development so that it results in, “no net loss of shoreline ecological function.” Ecological functions are outputs that provide organisms with a resource and are the result of interactions of ecological process and structural elements (Brennan & Culverwell 2004). For example a fish may require water in a narrow range of temperatures (water quality as ecological function), and the temperature, along with other water quality characteristics, may be regulated by shading (processes) provided by trees (structural elements). So to assess the ecological impact of proposed development projects, counties and cities must regularly monitor the configuration of small landscape structural elements within individual tax parcels and land use zones. This has proven to be very technically challenging to shoreline communities in Washington State (Clancy et al. 2009), but we believe this challenge can be met with accurate high resolution land cover maps can be produced inexpensively from aerial. For this study we applied state-of-the-art photogrammetry and land cover mapping techniques to a set of aerial photographs that have been acquired in early spring as part of a cooperative purchase agreement between shoreline cities and other agencies in King, Kitsap, and Snohomish counties in central Puget Sound.

1.1.1 Photogrammetry

Over the past 150 years photogrammetry tools and techniques have progressed through four distinct development phases, and each time access to the technology and the quality of data derived from it have improved dramatically (Linder 2009). This progression began with the plane table photogrammetry phase (1850-1900), during which specially trained surveyors oriented photos taken from the ground over existing maps, and transferred new measurements between objects from the photos to the maps. The photos were oriented based on previously surveyed points that are easily identifiable points in the photos known as Ground Control Points (GCP). The next phase, analog photogrammetry (1900-1960), is defined by the use of stereoscopy and aerial photos. Specially trained photogrammetrists were able to create the illusion of depth in photos by orienting and simultaneously viewing two overlapping photos, known as stereo photo pairs, taken of the same scene from slightly offset locations (Figure 3). Viewing and measuring stereo photo pairs was tedious and required expensive training and mechanical instruments, but facilitated continuous topographic mapping of areas that had been properly photographed. Photogrammetrists would typically trace apparent contour lines on aerial photos, and transfer those measurements to maps. Computers ushered in the era of analytical photogrammetry (1960-2000), allowing photogrammetrists to calculate and record distances with smaller, less expensive, and easier to handle equipment. However this type of work is limited by the speed of the operator and the size and quality of physical photo prints. The current phase of digital photogrammetry (2000-present) is characterized by the use of digital images and computer software which automates many tasks and requires little training, making photogrammetry faster and more accessible than ever before (Leberl & Thurgood 2004).

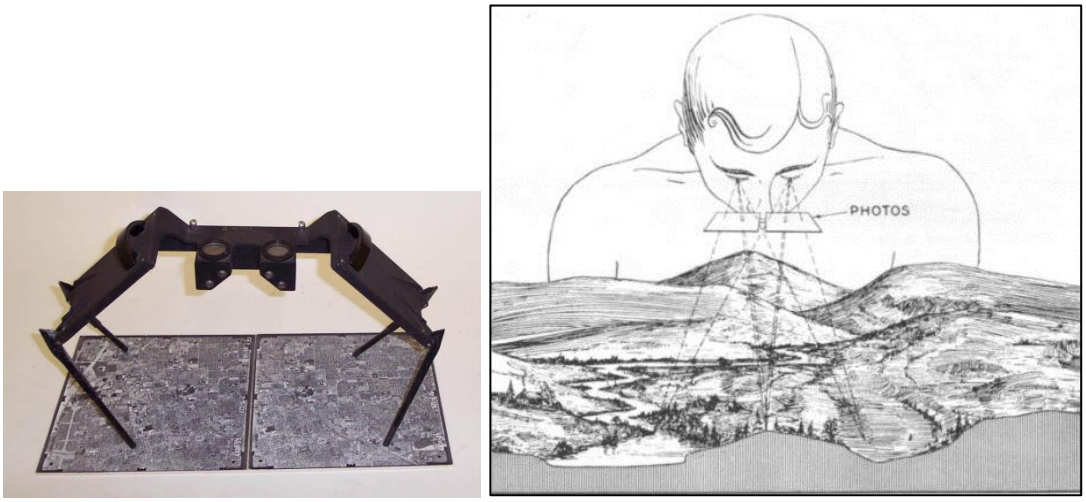

Figure 3. Stereoscopes (left, USGS 2014) allow a user to simultaneously view stereo photo pairs and create the illusion of depth. This mimics human vision (right,) by viewing objects from two different angles and resolving the two images into one 3D scene.

In this research we evaluated a versatile emerging digital photogrammetry method known as Structure from Motion (SfM) as implemented in the PhotoScan software by Agisoft (2013). Unlike conventional photogrammetry, many tasks in SfM are fully automated, allowing users to produce photogrammetric measurements rapidly, inexpensively, and with little training. Structure from Motion also differs from conventional photogrammetry in that it was developed for computer vision applications to reconstruct 3D scenes from photographs taken at different angles, and without a priori knowledge of camera pose or GCPs. This makes the technique particularly well suited to 3D photogrammetry of images taken from Unmanned Aerial Vehicles, which lack the accurate camera position and orientation data typically collected by a GPS unit and Inertial Measurement Unit during large scale aerial photography, but may be georeferenced through the use of GCPs if necessary (Honkavaara et al. 2009, Remondino 2011, Mathews & Jensen 2013, Lucieer et al. 2014, Goncalves & Henriques 2015).

The SfM workflow begins with identifying by areas in images known as “tie points” that are invariant between images to image scaling and rotation, and partially invariant to 3D camera

viewpoint and illumination conditions (Lowe 2004). The number of tie points detected in a scene is dependent on image texture and resolution, so complex images of high resolution will generate more tie points than homogenous images at low resolution (Snavely et al. 2007). Next camera and 3D object positions are estimated and optimized through "bundle adjustment," "bundles" of light rays originating from each tie point are "adjusted" iteratively to minimize error (Triggs et al. 2000). The result is a sparse "point cloud", a 3D array of modeled visible locations. The final step is incremental triangulation of 3D point positions, resulting in a dense point cloud from which object surfaces may be modeled.

That SfM is automated, inexpensive and easy-to-use make it potentially well-suited for the frequent monitoring required of cities and counties by the Shoreline Management Act. However the automated processes of SfM are known to fail at producing useful measurements in areas of low contrast such as sand and snow (Mancini et al. 2013, Fonstad et al. 2013), or areas occluded from stereoscopic viewing by steep slopes, vegetation, or shadows (Fabris & Pesci 2005, Lavernick et al. 2014). Therefore it is important to closely inspect and validate SfM measurements taken for the first time from photos of a particular resolution and texture before using the measurements in geospatial applications. While SfM has shown promising results in producing accurate high resolution DSMs and orthophotos of buildings (Nebiker et al. 2014), bare earth (Fonstad 2013, Javernick 2014), single trees (Hernandez-Clemente 2014), and low growing vegetation (Lucieer 2014, Turner 2014), no study has yet validated measurements of more than one of these types of objects from the same set of large aerial photographs.

1.1.2 Land Cover Mapping

Thematic land cover maps derived from aerial photography classify the tallest visible surface of a given location, and are one of the most common applications of remote sensing (Foody 2002). Land cover classification methods have advanced rapidly in recent years in order take advantage of improvements in the spatial, spectral, and temporal resolutions of DSMs and orthophotos. Historically, pixel-based methods were used to classify areas based on the radiometric data of a single pixel covering that area and may still be appropriate for datasets of low spatial resolution (>30m pixel) (Myint et al. 2011). Presently, Object Based Image Analysis (OBIA) is emerging as a more suitable option for images with high spatial resolution and high land cover heterogeneity (Hay & Castilla 2006, Blaschke et al. 2014). Object Based Image Analysis consists of first demarking areas of similar pixel values in an image, called image objects. Next an algorithm is developed to automatically assign objects to thematic classes based primarily on spectral statistics of the objects, as well as texture, shape, and contextual relationships to other areas. Object structural statistics may also be used when orthophotos are fused with DSMs and combined into a single, multiple band, raster dataset. Object Based Image analysis of orthophotos fused with DSMs derived from lidar data has consistently resulted in accurate comprehensive land cover mapping (Sohn & Dowman 2007, Erdody & Moskal 2010, McFaden et al. 2012, Styers et al. 2014), but very little OBIA has been conducted on orthophotos fused with DSMs derived from SfM. Previous research in this field has been of limited thematic extent, and has resulted in accurate high resolution maps of vegetation type (Debella-Gilo et al. 2013), vegetation physiology (Turner et al. 2014), and buildings (Nebiker et al. 2014). No

research has yet studied the suitability of orthophotos and DSMs derived from SfM for generating comprehensive land cover maps through OBIA.

1.2 Research Objectives

Structure from Motion is emerging as a suitable tool for inexpensively generating accurate high resolution landscape structural measurements from photographs, and the measurements may be suitable for use in comprehensive land cover mapping. However the accuracy and resolution of the measurements is dependent on the resolution and texture of the source photographs. The goal of this study was to improve understanding of the strengths and weaknesses of Structure from Motion in two ways:

1. Validate Structure from Motion measurements taken from high resolution aerial photos through production and analysis of Digital Surface Models and an orthophoto of a rural coastal peninsula.

2. Assess the accuracy of a land cover map of a rural coastal peninsula based on a Digital Surface Model and orthophoto generated using Structure from Motion.

2. Methods

2.1 Study Area

The study area is a ~400 hectare peninsula in the City of Bainbridge Island on the west side of the central Puget Sound in Washington State (Figure 4). The Puget Sound is the second largest estuary in the United States and is a fjord system of saltwater flooded glacial valleys fed by freshwater from the Olympic and Cascade Mountain watersheds (USGS 1946). Elevations within the study area range from sea level to 90 m; the terrain is especially steep on the face of the bluffs but otherwise consists of rolling hills and valleys.

Included in the study area are 6.5 km of shoreline that are varied in form and land use. The shore forms and their respective portions of the study area are: bluff backed beach 43%, rocky platform 20%, artificial construction 20%, one barrier lagoon 10%, one pocket beach 2%, one open coastal inlet <1% (PSNERP 2009). Land use zones established by the City of Bainbridge Island permit 2 residences per acre in most shoreline tax parcels in the area. The exceptions are on the northeast corner, where 4.3 houses per acre are permitted along a 500m length adjacent to for four large parcels transitioning from a former water dependent creosote plant and current EPA Superfund site to future parkland. The shoreline is habitat for deer, raccoons, fishes, birds, bivalves, and invertebrates. Eelgrass beds are present along the shore and provide refuge for salmon, spawning habitat for herring, and food for birds (Williams & Thom 2001, Williams et al. 2004)

Upland the land use consists of residential neighborhoods, second and third growth forest, agriculture, and parkland. City of Bainbridge Island zoning permits 0.4 or 1 residence per acre, with the exception of a 4.3 residence per acre zone in the northeast. The forest is

characteristic of Puget Sound lowland forests as described by Franklin & Dyrness (1988). It is comprised mostly of western hemlock (*Tsuga heterophylla*) and Douglas fir (*Pseudotsuga menziesii*), as well as western red cedar (*Thuja plicata*), bigleaf maple (*Acer macrophyllum*), red alder (*Alnus rubra*), and madrone (*Arbutus menziesii*) but has been altered by historic logging and other human development. Common shrubs in and near the forested areas include salal (*Gaultheria shallon*), sword fern (*Polystichum munitum*), and Pacific rhododendron (*Rhododendron macrophyllum*). There are presently non-native trees, shrubs, and groundcovers intentionally introduced in residential areas.

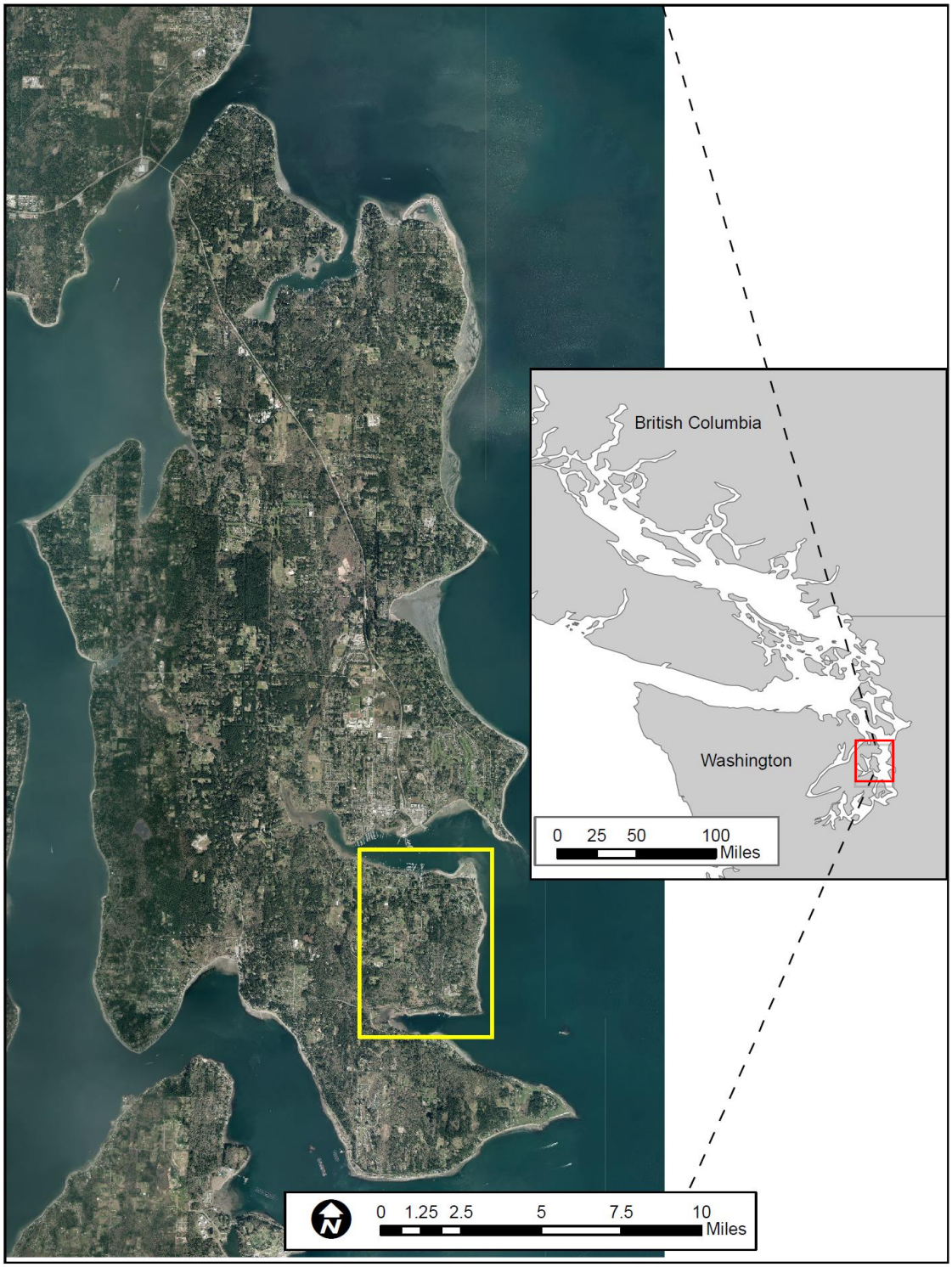

Figure 4. Study area outlined in yellow on Bainbridge Island, Washington, taken March 2012. Imagery acquired by Aeroquest Mapcon, provided courtesy of City of Bainbridge Island. Bainbridge Island outlined in red inset in central Puget Sound, WA.

2.2 Remotely Sensed Data

In this study our primary data consists of six 8-bit, four-band color infrared images covering 200 hectares each, acquired in March of 2012 (GSD = 0.15m). Figure 4 is an orthophotograph derived from this imagery using analytical photogrammetry techniques. We chose these photos due to the fact that they are part of a larger acquisition covering Kitsap, King, and Kitsap counties that has been purchased cooperatively between 90 public and private agencies since 2002, and results from study of this photo subset could be applicable to these large extents of space and time. It is important to note that these agencies currently highly prioritize visibility of roads under trees, and so they elect to have the imagery acquired in early spring when deciduous trees have the fewest leaves and daylight duration is increasing. This is important because the leaf-off condition of the plants is known to affect the resolution of SfM measurements of very high resolution photos (Dandois & Ellis 2013). The images were collected in a south to north transect, and each image overlaps the adjacent images by 50%. The imagery was acquired using a film camera, and the images were then digitally scanned. During the imagery acquisition flights, Aeroquest Mapcon simultaneously recorded the location of the plane when each photo was taken, using an Inertial Measurement Unit and GPS unit (King County 2015). In the study area Aeroquest Mapcon also used GPS units to record the locations of three Ground Control Points to be later identified in the aerial photos.

2.3 Digital Surface Model and Orthophoto Production

With Agisoft PhotoScan, we used the aerial photos, their positional data, and Ground Control Points, to produce an orthophoto and three Digital Surface Models (DSM, Figure 1): a Digital Height Model (DHM), Digital Terrain Model (DTM), and a normalized Digital Surface Model (nDSM). Though not necessary for scene construction, we began the workflow (Figure 5) by creating a 3D camera location model based on GPS data collected during the imagery acquisition flight so that the subsequent measurements would be georeferenced, a necessary condition for geospatial application to land cover mapping. The photos were then aligned using the bundle adjustment procedure based on camera locations and a sparse cloud of tie points, areas with similar appearances in adjacent photos. To improve vertical and horizontal alignment of the photos we then identified and mapped Ground Control Points using GPS data where visible in each photo. For the final step in the SfM process, scene geometry was incrementally triangulated, resulting in a three-dimensional dense point cloud of points visible between adjacent photos.

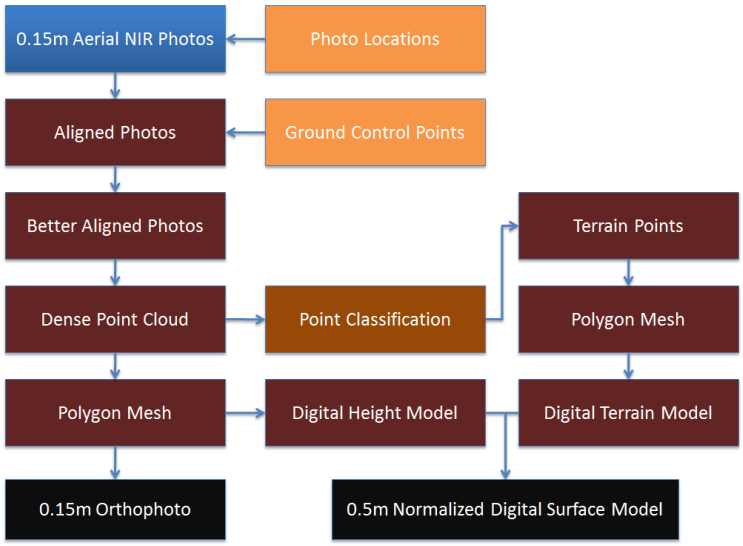

Figure 5. Workflow for generating orthophoto and normalized surface model using Agisoft Photoscan.

Next we used the dense point cloud to construct two polygon meshes and export the orthophoto and DSMs derived from those meshes. The first mesh was generated from the entire dense point cloud, aerial photos were then distorted to fit the mesh, stitched together and exported as a single orthophotograph. Next we used the existing polygon mesh to generate a DHM raster image showing the height above sea level of all pixels. We then returned to the dense point cloud and classified a subset of those points as terrain points. We used PhotoScan to classify terrain points by dividing the cloud into 100m cells, locating the lowest point in the cell, and selecting all points that are within 1m vertical distance of the lowest point, and then selecting any points adjacent to a terrain point and less than 15 degrees higher than the terrain point. We arrived at these parameters for terrain classification by trial and error, assessing their accuracy through visual inspection and comparison to the spectral data associated with the points. Once we had optimized the terrain classification through trial and error we used the terrain points to generate a polygon mesh and DTM raster image showing the height of the terrain above sea level. We then used ArcGIS (ESRI 2012) to subtract the DTM values from the DHM values to produce a nDSM raster image showing the heights of points above terrain level. To make the data suitable for OBIA we then fused the orthophoto with the nDSM, resulting in a single image raster composed of five bands of data: red, blue, green, and near infrared brightness values, and height above ground level for each pixel of the study area.

2.4 Resolution and Accuracy Assessment of Photogrammetry

To evaluate the horizontal and vertical resolution of the photogrammetric measurements we analyzed the data in two formats: the dense point cloud and DSMs derived from the point cloud. The dense point cloud allows us to evaluate differences in resolution by land cover type,

and the DSMs tell us the maximum resolution since areas of lower measurement resolution are interpolated to match the areas of the highest resolution. We calculated the density of the point cloud using FUSION (McGaughey 2009), and recorded the vertical and horizontal resolution of the DSMs from a report generated in ArcGIS.

We assessed the accuracy of the photogrammetric measurements of the terrain by comparing the DTM that we produced to the best available DTM for the same area, the National Elevation Dataset (NED) DTM (Figure 6, Gesch et al. 2002). The NED DTM was produced using analytical photogrammetry techniques in 2000, and is the highest resolution (2.3m GSD) continuous DTM that is freely available in the contiguous United States. In some areas the NED may be supplemented by manual editing and ground survey data. To determine the possible effects of topography on disagreement between the datasets, we subtracted the NED DTM data from the DTM we produced, and mapped the differences. To determine the magnitude of average disagreement we calculated the Root Mean Square Error between the two DTM datasets.

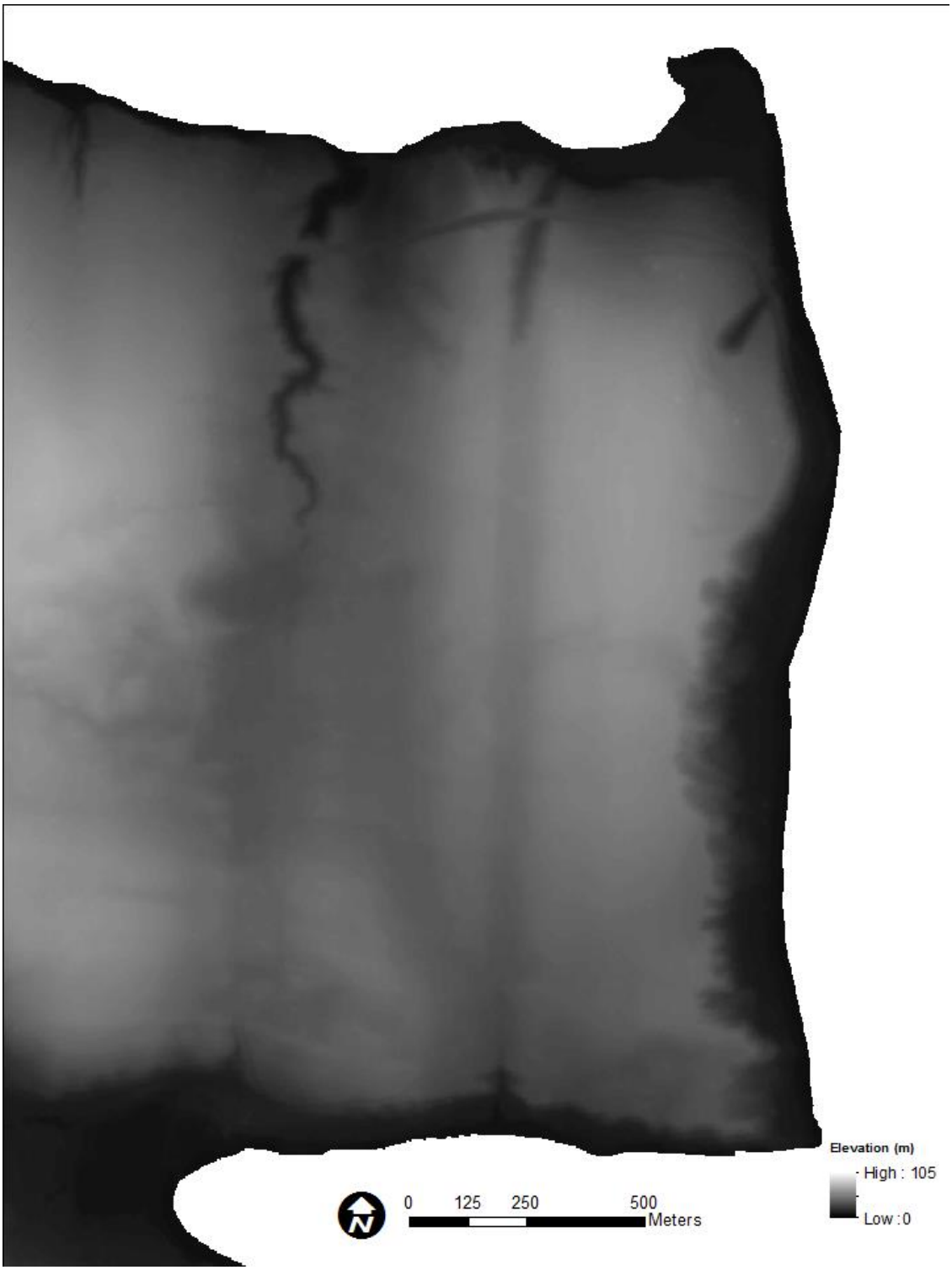

Figure 6. Digital Terrain Model of the study area on Bainbridge Island, WA. Elevation above sea level is symbolized as black (sea level) to white (105m above sea level). (National Elevation Dataset, Gesch et al. 2002)

We qualitatively assessed the accuracy of the shape of the above ground objects through close visual comparison of the orthophoto and DHM. We evaluated the accuracy of the photogrammetric measurements of trees and buildings by comparing heights derived from the nDSM we produced to the heights of the same trees and objects as measured by a laser rangefinder (error of ±0.3m). The comparison consists of simple linear regression analyses and calculation of the coefficients of determination, which indicate how well the nDSM determines the heights of the objects we measured. We selected the trees and buildings and trees in the field and attempted to sample an even distribution across heights, shapes, position in the study site, and surrounding landscape type.

2.5 Land Cover Classification Using Object Based Image Analysis

We used eCognition by Trimble to develop an algorithm for semi-automatically classifying the pixels of the fused orthophoto and nDSM. The workflow (Figure 4) begins with segmenting the fused imagery into image "objects" of interest. Of the many segmentation algorithms available in eCognition we chose the multiresolution segmentation since it hierarchically aggregates objects at different scales, and the land cover categories we were attempting to map are of different sizes and textures. We based our segmentation on the red, green, blue, and near infrared brightness values, as well as the nDSM, and weighted the infrared brightness at twice that of the other values since it showed high contrast between vegetation, a critical structural element indicator for evaluating shoreline ecological function, and other classes. The heterogeneity of the pixel values within image objects is defined by the "scale" factor, a higher value of this parameter results in fewer, more heterogeneous objects with a larger average size. In eCognition image objects may also be delineated based on their geometric properties, and the weight of this factor is controlled by the "shape" and "compactness" parameters. Selecting the optimal values for these parameters is inherently subjective and requires close visual inspection of different combinations through trial and error. The smallest objects we sought to classify are individual shrubs and we found that the best combination of parameters to segment them and other classes was to set the scale parameter to 25, the shape parameter to 0.1, and the compactness parameter to 0.5.

We classified the segmented image objects based first on spectral, then structural, and finally contextual criteria determined by logical values, image interpretation and inspection, and two-dimensional feature space plots using a modified version of the algorithm developed by

Styers et al. (2014) (Figure 7). Knowing that water absorbs near infrared reflectance we began with classifying areas with a high ratio of blue to low near-infrared brightness as marine water. Next, areas with low mean brightness (the mean of the red, green, blue, and near-infrared bands) were temporarily classified as shaded, then reclassified based on height and the Normalized Difference Vegetation Index (NDVI, Tucker 1979) into all classes except water and impervious surfaces. We then temporarily classified all vegetation together based on mean NDVI > 0.01, and then into vegetation classes based on height. Areas with high brightness (mean > 195) were initially classified as buildings, and then flat areas within that classification (mean nDSM < 1m) were reclassified as impervious surfaces. Next the remaining areas with a blue brightness (mean > 150) were classified as impervious surfaces, and bare ground was classified by a near-infrared reflectance threshold (mean < 200). We noted at this stage that many areas of bare ground had been misclassified as impervious surfaces; they were often adjacent to one another and were especially common on the beaches. So we merged the impervious surfaces and reclassified areas larger than 8000 pixels as bare ground. Some small patches of bare ground areas remained classified as impervious surfaces, so we segmented the impervious surfaces using a multiresolution quadtree segmentation with a scale parameter of 60, which creates square segments of various sizes based solely on spectral heterogeneity. We then classified all impervious surfaces with NDVI > -0.08 as bare ground, and merged all bare ground objects. At this point we had inadvertently reclassified some impervious surfaces as bare ground, and so segmented bare ground with another quadtree segmentation a scale parameter of 60. The resulting image objects with NDVI > -0.08 were reclassified as bare ground. Finally, all objects

that shared more than 60% of their border with a segment classified as building were reclassified as building.

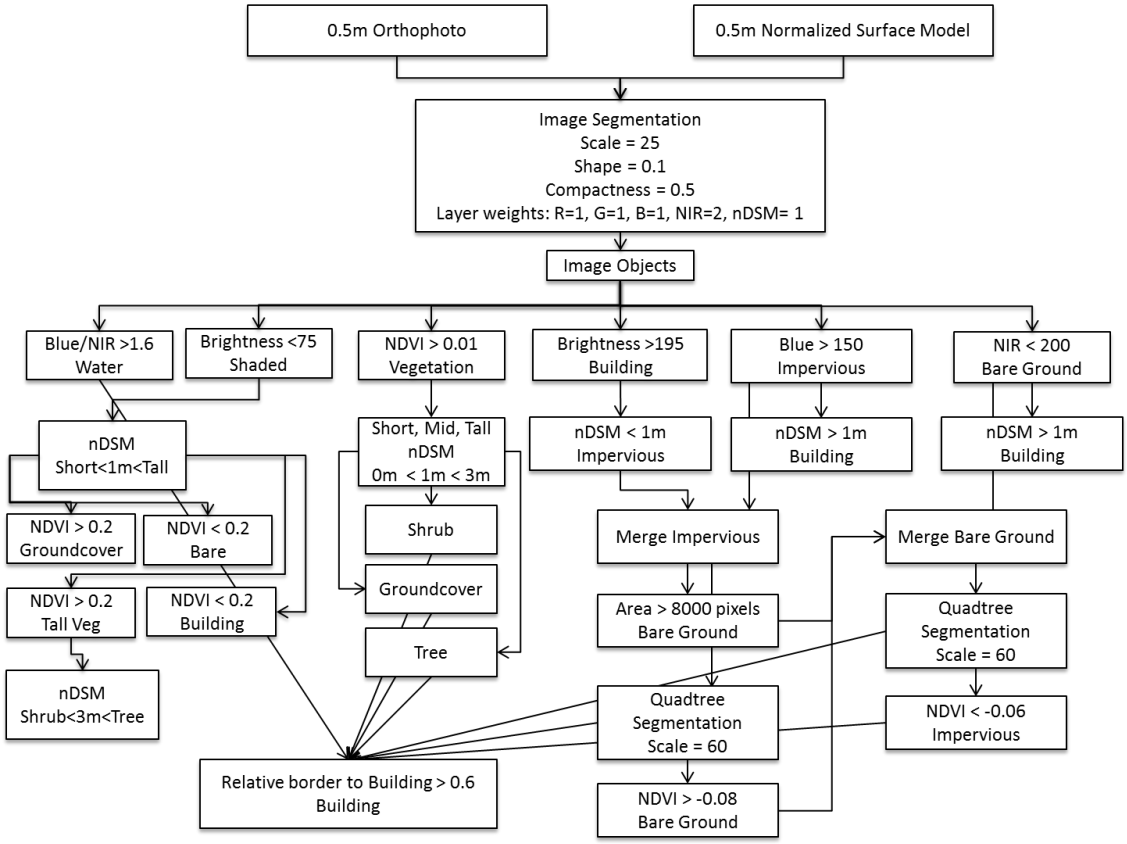

Figure 7. Workflow for segmenting and classifying orthophoto and nDSM into thematic land cover categories using eCognition.

2.6 Land Cover Accuracy Assessment

We assessed the accuracy of the land cover classification algorithm in the typical fashion, comparing the reported land cover of randomly selected points to the actual land cover, and generated a confusion matrix which reports how well the algorithm classified the imagery (Foody 2002). We first randomly placed 331 accuracy assessment points proportionally by total land cover area of each class as reported by the land cover map. We then manually classified

each point by inspecting the nDSM and color infrared orthophoto in the same location and assigning the point to a class based on standard definitions of the classes (Table 1).

Table 1. Land cover classification descriptions.

Class	Description
Bare ground	Soil lacking vegetation
Buildings	Built up structure over 1m tall
Groundcover	Plant that does not grow above 1m tall
Impervious	Terrain level surface that does not permit water to permeate
Shrub	Plant that may grow to between 1m and 3m tall
Tree	Plant that may grow above 3m tall
Water	Body of water at least $1m^2$

3. Results & Discussion

3.1 Photogrammetry Resolution and Accuracy

The horizontal resolution of the SfM measurements that we generated from aerial photos is generally very high. The maximum density of the point cloud is 5 points/m^2, with some small "holes" and areas of lower density where points were not well detected. From this dense point cloud we generated DSMs with 0.5m GSD, much higher resolution than the 2.3m GSD of the NED DTM, the previously highest resolution DSM available for the same area (Gesch et al. 2002). It is also notable that PhotoScan is capable of producing DSMs at even higher resolution, but with larger holes in the point cloud. Thus there is a tradeoff between resolution and continuity which has not been reported in other studies using PhotoScan. Holes in the point cloud are evident in derived DSMs as smooth interpolated areas lacking useful elevation data (Figure 8), making them less suitable for land cover mapping through OBIA.

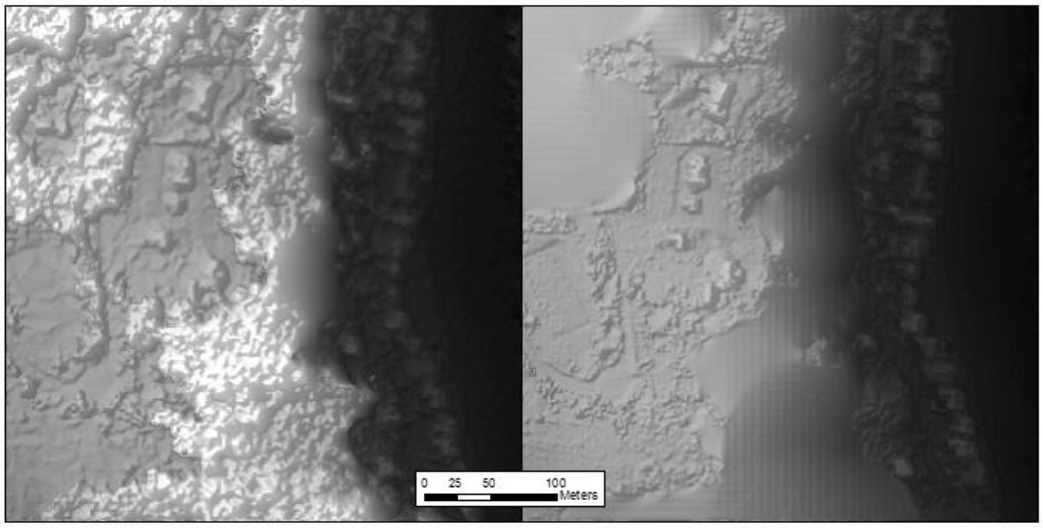

Figure 8. DHMs derived from medium (left, 0.5m GSD) and very high (right, 0.15m GSD) density point clouds generated in PhotoScan.

The holes in the point cloud are most common in dense forest canopy and on steep slopes, which is consistent with the results of application of SfM to other forested areas (Zebedin et al. 2006,

Dandois & Ellis 2013) and steep slopes (Fabris & Pesci 2005). On the other hand it is surprising to note that shaded areas which are common in the photos were consistently triangulated, perhaps due to the very high resolution of the source photos.

The average point density of the entire point cloud of SfM measurements including the holes is 4 points/m^2, which is similar to a typical aerial lidar data set. This has exciting implications for the utility of SfM measurements in many applications, as lidar data of 4 points/m^2 density has been shown to be suitable in geology (Collins & Sitar 2008, Cavalli et al. 2008), urban planning (Lohani & Singh 2008, Chen et al. 2008), fire modeling (Anderson et al. 2006, Wang & Glenn 2009) and forestry (Suratno 2009, Reutebuch et al. 2003). However unlike lidar the points we triangulated are not evenly distributed, and lidar can potentially penetrate the upper surfaces of vegetation in a given horizontal location and measure several heights, including terrain under vegetation. The vertical resolution of the DSMs produced from SfM and the NED DTM are both extremely high, yet the utility of these data is limited by their error. Elevations derived from SfM DSMs are reported in the picometer range (0.0000000000001m) with a Root Mean Square Error (RMSE) of 1.09m, the NED DTM reports data in the nanometer range (0.0000000001m), with RMSE = 1.55m.

Comparison of the DTM that we produced (Figure 9) to the National Elevation Dataset DTM (Figure 6) shows that the DTM we produced is fairly accurate (RMSE =3.29), with some notable exceptions. There are several locations in the study area with an absolute difference between the DTMs greater than 6m (Figure 10). All of these areas (for example the bluff face in the southeast corner and stream channel in the northwest quadrant) consist of complex

topography under dense tree canopy where terrain points were not detected, resulting in holes in the point cloud that were interpolated as flat surfaces.

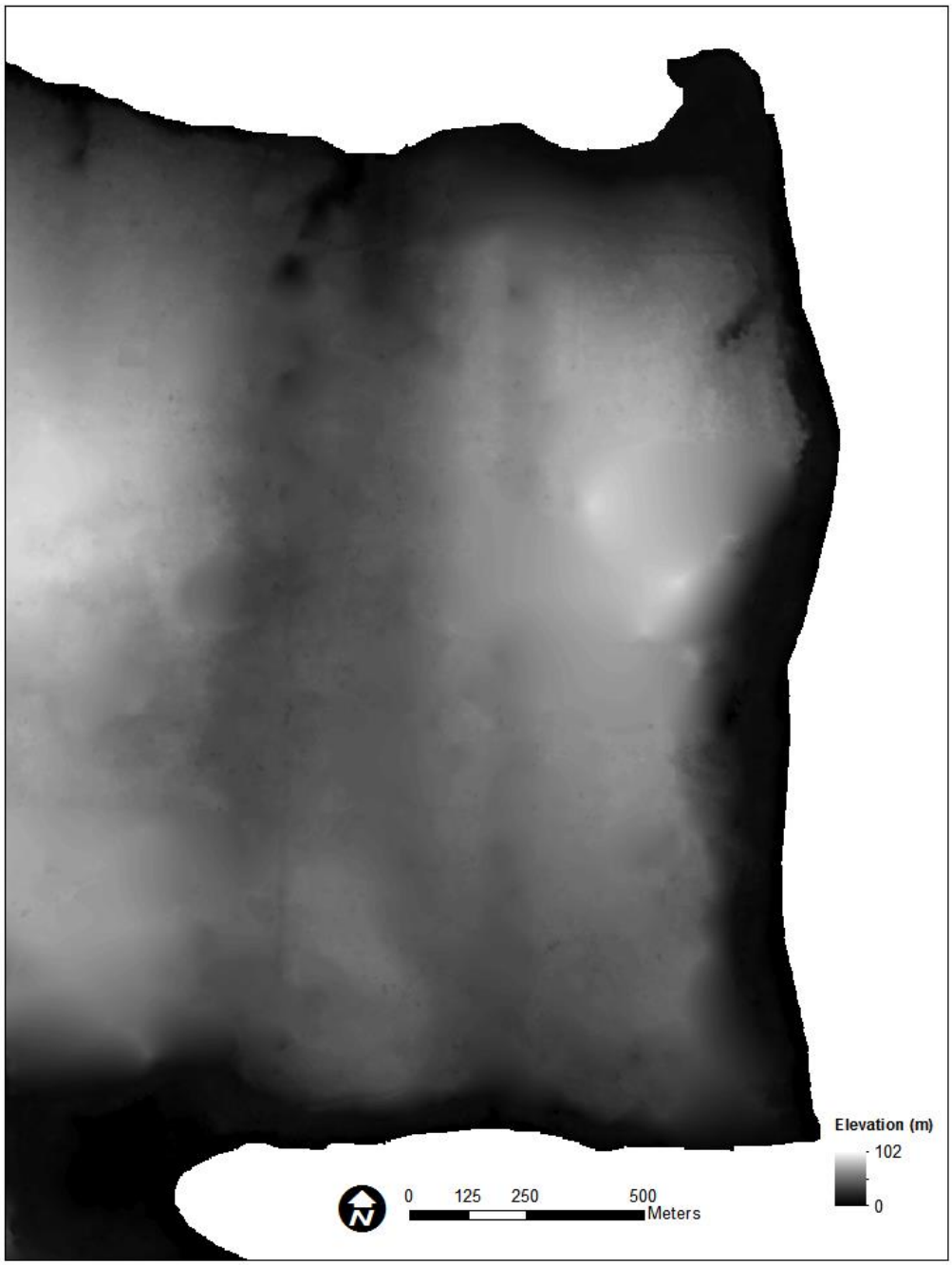

Figure 9. Digital Terrain Model of Bill Point produced using aerial photos and Agisoft PhotoScan.

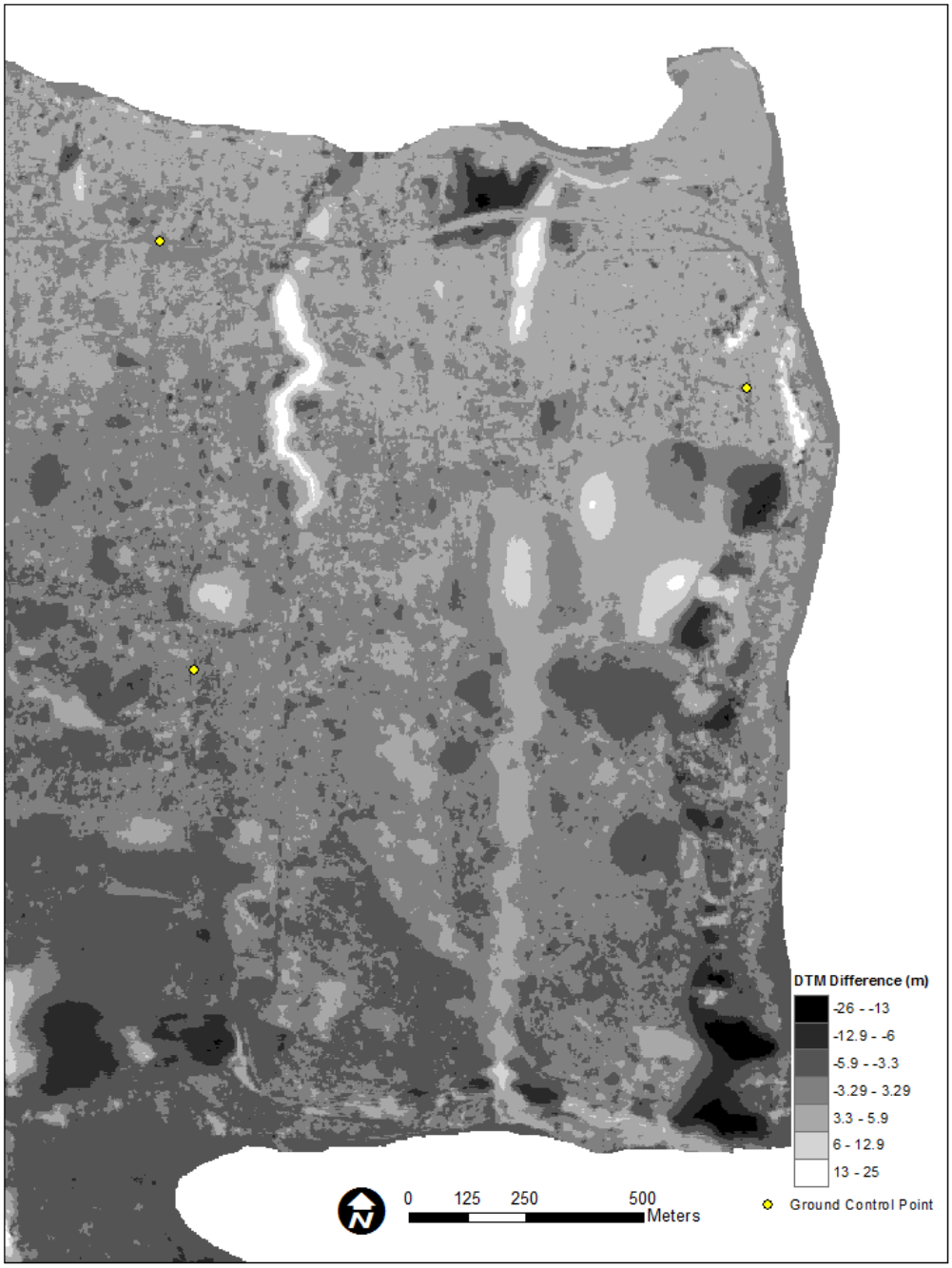

Figure 10. National Elevation Dataset DTM subtracted from DTM produced with PhotoScan to show difference between the datasets. Ground Control Points recorded using a GPS unit by King County staff.

The normalized Digital Surface Model (nDSM, the difference between the upper Digital Surface Model and the Digital Terrain Model) (Figure 11), produced accurate results for tall objects, but failed to detect the heights of several trees that we measured with a laser rangefinder. Linear relation between the heights of buildings measured with a laser rangefinder and the heights of the same buildings measured with the nDSM displays a R^2 of 0.80, along an equation: y=1.08x-1.19 (Figure 12). This coefficient and equation, and the fact that the data do not appear to be heteroscedastic, indicate that the nDSM consistently slightly underestimates building heights within the range of heights we sampled. Linear relation of heights of trees measured in the same ways displays a R^2 of 0.46, along an equation: y=0.72x-2.61 (Figure 13). Besides six trees whose heights were severely underestimated, the nDSM appears to have also consistently and slightly underestimated the heights of trees. The six trees that were severely underestimated either had very narrow crowns or were leaf-off deciduous trees.

Tree height validation is complicated by the fact that the trees were measured using a laser rangefinder (error of ±0.3m) three years after they were photographed, so they may have grown, been trimmed, or lost height due to breakage from strong winds. For the trees and buildings both, we measured heights that could be taken from public property with a laser rangefinder, which biases the results towards objects in open areas that may be more easily detected by dense image matching. Notably we were not able to take measurements where there is high difference between our DTM and the NED DTM (complex and steep terrain under contiguous tree canopy), where the heights of trees measure up to 77m and are clearly exaggerated (Figure 11).

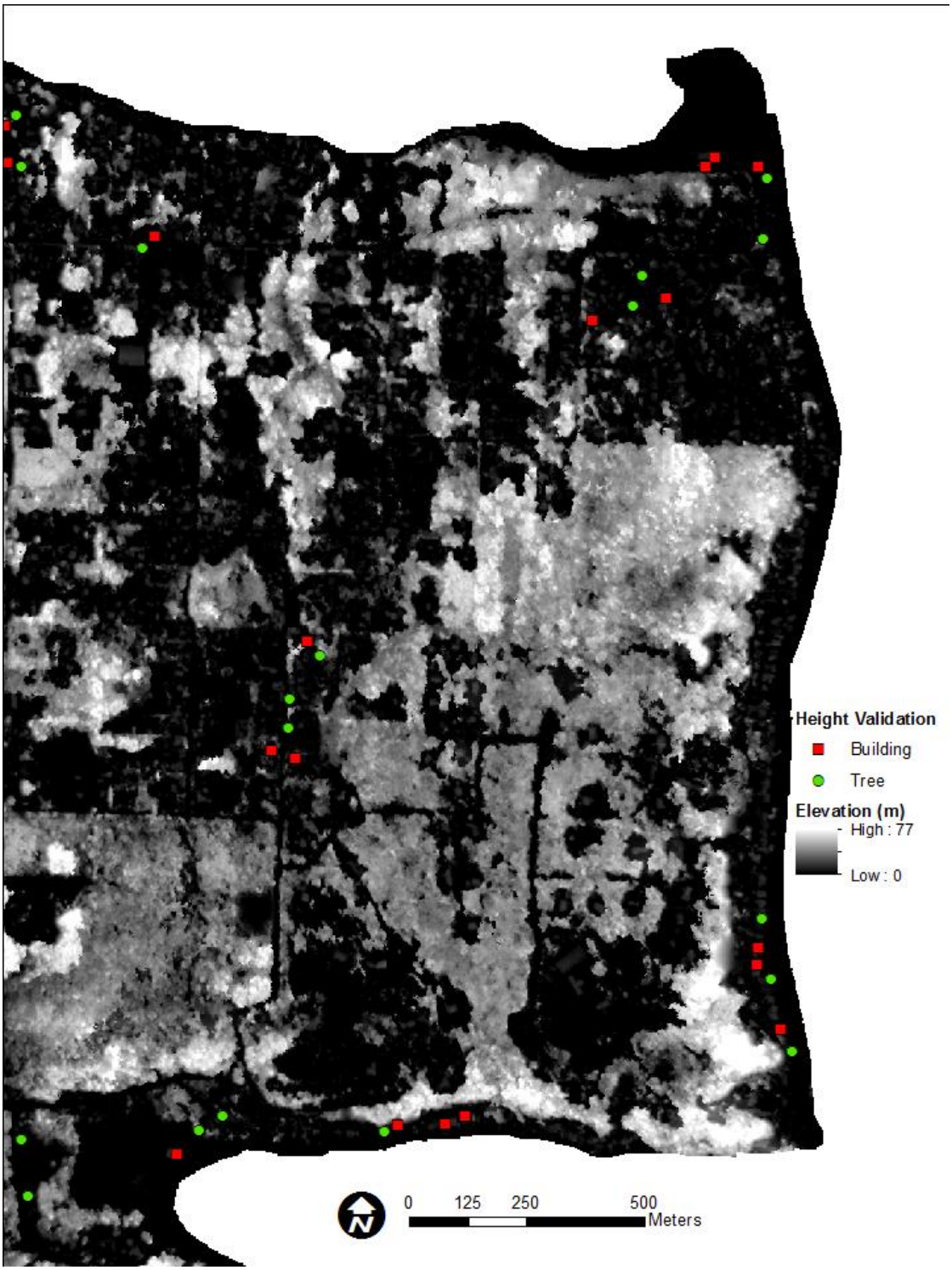

Figure 11. Normalized Digital Surface Model, produced by subtracting the DTM elevations from the DHM elevations produced with PhotoScan.

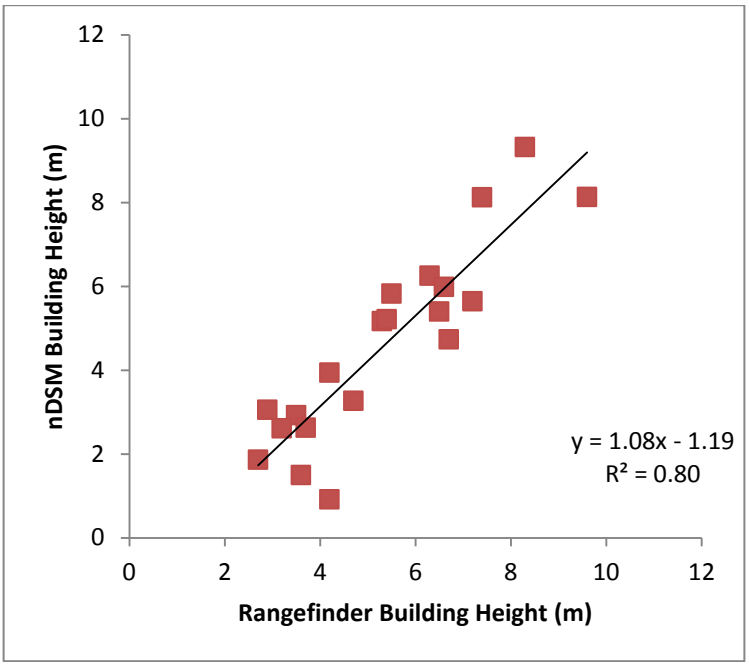

Figure 12. Linear regression model comparing building heights measured by laser rangefinder and the normalized Digital Surface Model produced with PhotoScan.

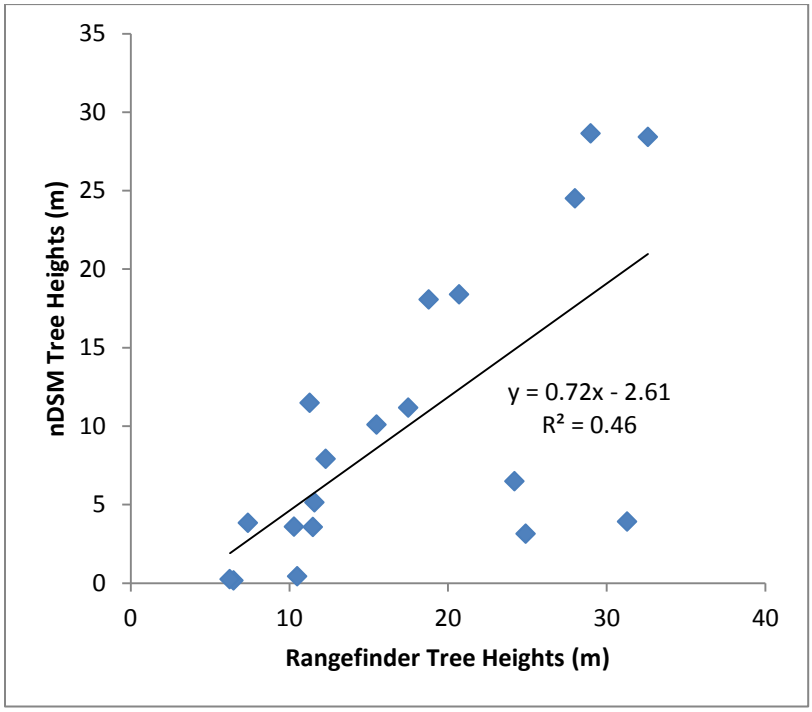

Figure 13. Linear regression model comparing tree heights measured by laser rangefinder and the normalized Digital Surface Model produced with PhotoScan.

The DHM that we produced appears to accurately map the shape of most objects that we inspected, and the orthophoto that we produced is of high spatial resolution (0.15m GSD) and appears to fit the DHM well (Figure 14). Relative to DHMs produced from lidar data, ours does not appear to accurately map vertical surfaces such as the sides of buildings; instead it often maps them as a steep slope. It is more difficult to assess the texture of the heights of trees modelled by the DHM, but if they are accurate we believe they could be used to estimate tree biomass, similar to the work done by Dandois & Ellis (2013) and the large body of work using lidar models to do so (Zolkos et al. 2013).

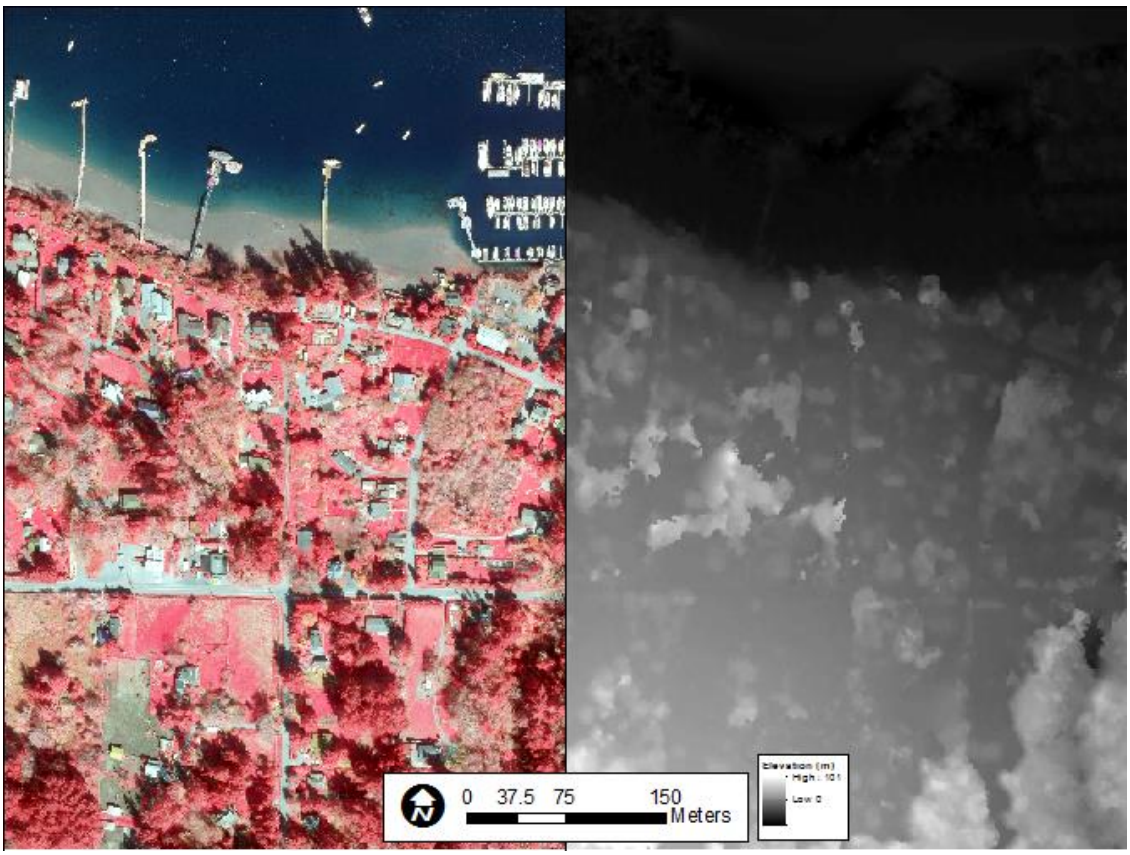

Figure 14. False color near infrared orthophoto (left) that has been fitted to the DHM (right).

3.2 Land Cover Mapping

The accuracy of the land cover map derived through OBIA of the fused orthophoto and nDSM is of high accuracy, with some confusion between spectrally and structurally similar classes that is common with the OBIA technique. The map is of much higher resolution (GSD = 0.5m) (Figures 15 & 16) than the National Land Cover Database (GSD = 30m), the best available land cover map of the same area (Homer et al. 2012). It appears to be very accurate, except for confusion between impervious surfaces and bare ground which are structurally and spectrally similar, and are commonly confused in automated land cover classification (Myint & Gober 2011, MacFaden et al. 2012, Weng 2012, Styers et al. 2014). Though we implemented a "clean-up" procedure with quadtree segmentations and reclassification, large sections of road are still classified as bare ground, and some sections of beach are classified as impervious surfaces. It may be that the lighting conditions have exacerbated this problem, as the average brightness of the scene is low, and spectral signatures are more similar than they would be had the photos been acquired on a brighter day. Solving this problem is especially important to users interested in applying this method to SMP administration. Similarly we overlooked accurate detection of small bodies of freshwater after having successfully classified marine water, and correcting this oversight is important, but difficult due to the spectral similarity of the small ponds and wetlands to impervious surfaces. The large areas on the east facing shoreline classified as groundcover also merit further study. Eelgrass beds are known to be present in the area, but there is also dark exposed bedrock with a spectral signature similar to plants that has been classified as groundcover and may in fact be covered in algae. Expanding the categorical resolution of the land cover map to include intertidal areas and aquatic vegetation is a technical challenge that we

did not pursue, but aquatic vegetation has been classified successfully using imagery alone (Moskal et al. 2011), and intertidal areas have been classified using imagery and lidar with limited success (Styers et al. 2014). Aquatic vegetation at least could likely be accurately classified using contextual filters (relative border to water or bare ground), and would certainly improve the utility of the map in SMP administration. In terms of SMP utility, it is also noteworthy that the map appears to have done a fairly good job of identifying overwater structures on the north and south facing shorelines.

The statistical accuracy assessment of the land cover map indicates that the map is indeed overall very accurate, and that most individual classes perform well. The overall accuracy is determined by dividing the total number of correctly classified points by the total number of points assessed; in this case the map is 86% accurate (Table 2). Of the 44 points that were classified incorrectly, 26 were vegetation points that were misclassified as other types of vegetation. Vegetation was first classified by spectral characteristics, and then assigned to a subclass based on height, and the largest source of confusion within vegetation is shrubs that have been misclassified as trees or groundcover. This indicates that the nDSM derived from SfM does not always accurately measure the height of shrubs. However the vegetation accuracies are generally high despite the fact that the leaf-off condition is known to cause confusion (MacFaden et al. 2012). The high accuracies of the vegetation classes indicate that the methods we have tested are useful for measuring the shape and extent of vegetation buffers which are an important element of managing land use to preserve shoreline ecological function (Brennan 2007). As we have discussed, spectral similarity to other bare ground is responsible for some of the poor performance of impervious surface classification (38% producer's accuracy) but it also appears

that SfM has failed to correctly map the heights of some building points and consequently they have been classified as impervious surfaces. It is exciting to note that 93% of the tree classification is correct, again indicating that SfM may potentially be very useful in forestry applications. Finally, the accuracy of the map could be improved through manual classification, which can be a cost-effective way to address confusion errors that me be impossible to resolve through automated filters (Styers et al. 2014).

The KHAT coefficient of agreement was developed to facilitate comparison between mapping projects by comparing the actual agreement (diagonal in bold in Table 2) to chance agreement determined by row and column totals. In this case KHAT=0.80 and is considered a "good" result (Lillesand & Kiefer 2012). Our results compare well with land cover maps derived from orthophotos and lidar in Olympia, WA (KHAT=0.79) (Styers et al. 2014), imagery alone in Seattle, WA (KHAT=0.75) (Moskal et al 2011), and imagery and a DSM derived from SfM in Norway (KHAT=0.65) (Debella-Gilo et al. 2013).

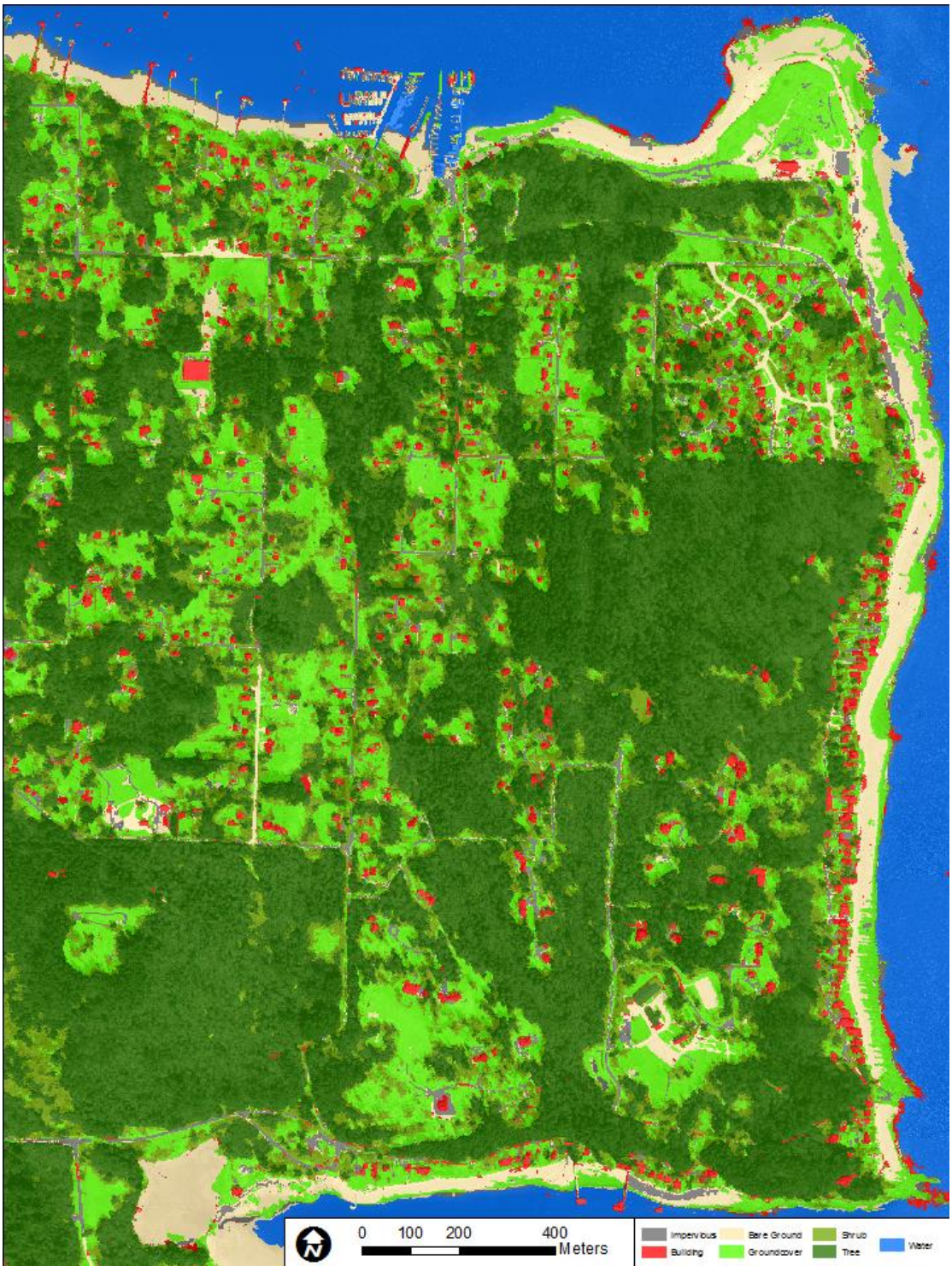

Figure 15. Land cover map of the study area based on Object Based Image Analysis of fused orthophoto and nDSM (0.5m GSD). The orthophoto is displayed underneath the land cover classification.

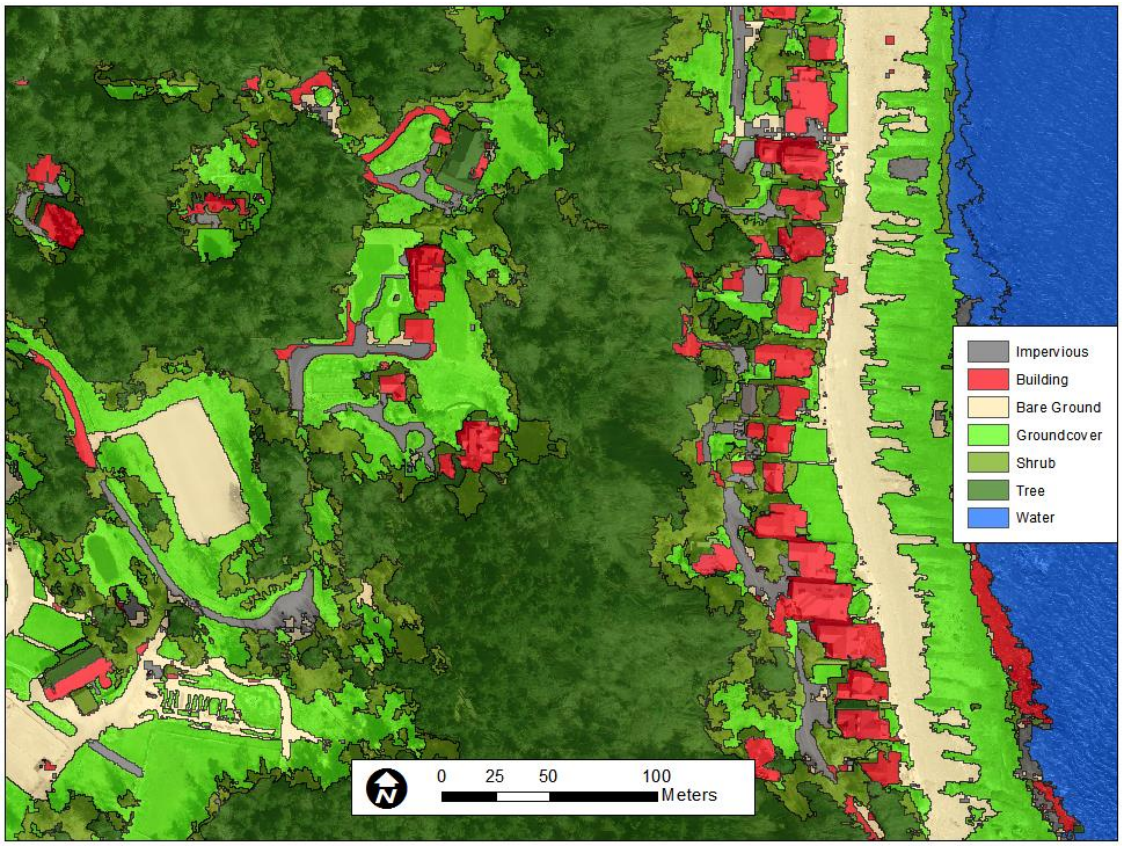

Figure 16. Land cover map (0.5m GSD) produced through OBIA of fused near infrared orthophoto and nDSM.

Table 2. Land cover map confusion matrix. Figures in bold on the diagonal axis are the number of points correctly classified in each thematic category.

		Map Classification							
		Tree	Shrub	Ground cover	Building	Impervious	Bare ground	Total	User's Accuracy
Photo Interpretation	Tree	**168**		2	1	1		172	98%
	Shrub	8	**27**	10	4	2	1	52	52%
	Groundcover	3	3	**58**				64	91%
	Building				**9**	3		12	75%
	Impervious			1	1	**6**	1	9	60%
	Bare ground					4	**18**	22	75%
Total		179	30	71	15	16	20	331	
Producer's Accuracy		93%	90%	82%	60%	38%	90%		

Overall Accuracy = 86%

KHAT = 80%

4. Conclusions

This study shows that SfM can produce accurate high resolution measurements of a coastal environment from high resolution aerial infrared photos. We confirmed that SfM may in some cases fail to accurately map complex terrain and tree canopy, but found that despite these errors the data is suitable for producing accurate land cover maps. This emerging technique shows great promise for many geospatial applications, particularly high temporal and spatial monitoring of land cover in order to preserve ecological function.

4.1 Trade-offs: Cost versus Accuracy

Digital photogrammetry may emerge as a low cost alternative to the type of landscape structural data typically acquired by lidar (stereophoto acquisition of the entire 80km^2 of Bainbridge Island, WA at 0.15m GSD was recently quoted at $19,000, and $27,000 for lidar of 8 points/m^2 density). Though it cannot be guaranteed to provide equivalently continuous data, SfM is capable of producing higher resolution data than a typical lidar acquisition over large areas. We also found that the PhotoScan dense image matching algorithm performs poorly when reconstructing dense canopy, an area where lidar excels, and lidar also outperforms SfM in terrain detection (Tarolli 2014). However the fact that SfM is well suited to producing DSMs from imagery acquired with UAVs is sure to make it a very economical choice for many applications (Remondino 2011).

4.2 Future Research

We believe that this land cover map is of sufficient accuracy, resolution, and ease of use to regularly monitor and study the effects of the presence of landscape structural elements on

ecological functions. Shoreline communities in Washington State could potentially improve the utility of the method we have developed here by first acquiring a more continuous and perhaps more accurate DTM from lidar data and subsequently monitor the changes in above-ground structures using SfM. This could result in thousands of dollars in savings as opposed to frequently acquiring lidar and effectively paying for a new DTM more frequently than is likely necessary. For this reason future research should be directed at the compatibility of above-ground SfM measurements and lidar based DTMs. Researchers should also exploit the availability of this high resolution characterization of the landscape to look for new insights into the effects of land cover and composition on shoreline ecosystems and answer some of the most pressing questions that land managers face when attempting to ensure no net loss of ecological function.

Bibliography

Agisoft, L., & PhotoScan, A. (n.d.). Professional Edition, Version 1.0. 0, 2013. Retrieved from https://scholar.google.com/scholar?q=agisoft+photoscan&btnG=&hl=en&as_sdt=0%2C48#6

Anderson, H. (2006). The use of high-resolution remotely sensed data in estimating crown fire behavior variables. Final Report to the Joint Fire Science Program. Retrieved from https://scholar.google.com/scholar?q=The+use+of+high+resolution+remotely+sensed+data+in+estimating+crown+fire+behavior+variables&btnG=&hl=en&as_sdt=0%2C48#0

Blaschke, T., Hay, G., Kelly, M., & Lang, S. (2014). Geographic object-based image analysis–towards a new paradigm. *ISPRS Journal of …*. Retrieved from http://www.sciencedirect.com/science/article/pii/S0924271613002220

Brennan, J., & Culverwell, H. (2004). *Marine Riparian: An assessment of riparian functions in marine ecosystems*. Retrieved from http://albergstein.com/cao/CAO Committee Recommendation Files/Fish and Wildlife Habitat Conservation Areas/Marine/brennan et al 2005 - marine riparian function.pdf

Brennan, J. (2007). Marine riparian vegetation communities of Puget Sound. Retrieved from http://oai.dtic.mil/oai/oai?verb=getRecord&metadataPrefix=html&identifier=ADA478100

Brennan, J., Culverwell, H., Gregg, R., & Granger, P. (2009). Protection of marine riparian functions in Puget Sound, Washington. *Washington Department of Fish and …*. Retrieved from https://scholar.google.com/scholar?hl=en&q=protection+of+marine+riparian+functions+in+puget+sound&btnG=&as_sdt=1%2C48&as_sdtp=#3

Chen, L., & Teo, T. (2008). Shaping polyhedral buildings by the fusion of vector maps and lidar point clouds. *… Engineering & Remote …*. Retrieved from http://www.ingentaconnect.com/content/asprs/pers/2008/00000074/00000009/art00006

Clancy, M., Logan, I., & Lowe, J. (2009). Management measures for protecting and restoring the Puget Sound Nearshore. *Olympia, Washington: Puget …*. Retrieved from https://scholar.google.com/scholar?q=Management+Measures+for+Protecting+and+Restoring+the+Puget+Sound+Nearshore&btnG=&hl=en&as_sdt=0%2C48#0

Collins, B., & Sitar, N. (2008). Processes of coastal bluff erosion in weakly lithified sands, Pacifica, California, USA. *Geomorphology*. Retrieved from http://www.sciencedirect.com/science/article/pii/S0169555X07004527

Crooks, G. (1973). Washington Shoreline Management Act of 1971, The. *Wash. L. Rev.* Retrieved from http://heinonlinebackup.com/hol-cgi-bin/get_pdf.cgi?handle=hein.journals/washlr49&section=20

Dandois, J. P., & Ellis, E. C. (2013). High spatial resolution three-dimensional mapping of vegetation spectral dynamics using computer vision. *Remote Sensing of Environment*, *136*, 259–276. http://doi.org/10.1016/j.rse.2013.04.005

Debella-Gilo, M. (2013). Object-Based Analysis of Aerial Photogrammetric Point Cloud and Spectral Data for Land Cover Mapping. *… Archives of the …*. Retrieved from http://www.int-arch-photogramm-remote-sens-spatial-inf-sci.net/XL-1-W1/63/2013/isprsarchives-XL-1-W1-63-2013.pdf

Erdody, T., & Moskal, L. (2010). Fusion of LiDAR and imagery for estimating forest canopy fuels. *Remote Sensing of Environment*. Retrieved from http://www.sciencedirect.com/science/article/pii/S0034425709003277

Fabris, M., & Pesci, A. (2005). Automated DEM extraction in digital aerial photogrammetry: precisions and validation for mass movement monitoring. *Annals of Geophysics*. Retrieved from http://www.earth-prints.org/handle/2122/1126

Fonstad, M. A., Dietrich, J. T., Courville, B. C., Jensen, J. L., & Carbonneau, P. E. (2013). Topographic structure from motion: a new development in photogrammetric measurement. *Earth Surface Processes and Landforms*, *38*(4), 421–430. http://doi.org/10.1002/esp.3366

Foody, G. M. (2002). Status of land cover classification accuracy assessment. *Remote Sensing of Environment*, *80*(1), 185–201. http://doi.org/10.1016/S0034-4257(01)00295-4

Gesch, D., & Oimoen, M. (2002). The national elevation dataset. *Photogrammetric …*. Retrieved from http://topotools.cr.usgs.gov/pdfs/gesch_chp_4_nat_elev_data_2007.pdf

Gomez, C., Hayakawa, Y., & Obanawa, H. (2015). A study of Japanese landscapes using structure from motion derived DSMs and DEMs based on historical aerial photographs: New opportunities for vegetation monitoring and diachronic geomorphology. *Geomorphology*. http://doi.org/10.1016/j.geomorph.2015.02.021

Gonçalves, J. A., & Henriques, R. (2015). UAV photogrammetry for topographic monitoring of coastal areas. *ISPRS Journal of Photogrammetry and Remote Sensing*, *104*, 101–111. http://doi.org/10.1016/j.isprsjprs.2015.02.009

Hay, G., & Castilla, G. (2006). Object-based image analysis: strengths, weaknesses, opportunities and threats (SWOT). *Proc. 1st Int. Conf. OBIA*. Retrieved from http://www.isprs.org/proceedings/xxxvi/4-c42/Papers/OBIA2006_Hay_Castilla.pdf

Hernández-Clemente, R., Navarro-Cerrillo, R., Ramírez, F., Hornero, A., & Zarco-Tejada, P. (2014). A Novel Methodology to Estimate Single-Tree Biophysical Parameters from 3D Digital Imagery Compared to Aerial Laser Scanner Data. *Remote Sensing*, *6*(11), 11627–11648. http://doi.org/10.3390/rs61111627

Honkavaara, E., Arbiol, R., & Markelin, L. (2009). Digital airborne photogrammetry—A new tool for quantitative remote sensing?—A state-of-the-art review on radiometric aspects of digital photogrammetric images. *Remote Sensing*. Retrieved from http://www.mdpi.com/2072-4292/1/3/577

Jancso, T., & Melykuti, G. (2011). Comparison of Digital Terrain Models gained by different technologies. In *Proceedings 2011 IEEE International Conference on Spatial Data Mining and Geographical Knowledge Services* (pp. 324–329). IEEE. http://doi.org/10.1109/ICSDM.2011.5969056

Javernick, L., Brasington, J., & Caruso, B. (2014). Modeling the topography of shallow braided rivers using Structure-from-Motion photogrammetry. *Geomorphology*, *213*, 166–182. http://doi.org/10.1016/j.geomorph.2014.01.006

Lane, S. N., James, T. D., & Crowell, M. D. (2000). Application of Digital Photogrammetry to Complex Topography for Geomorphological Research. *The Photogrammetric Record*, *16*(95), 793–821. http://doi.org/10.1111/0031-868X.00152

Leberl, F., & Thurgood, J. (2004). The promise of softcopy photogrammetry revisited. *… Archives of the Photogrammetry, Remote Sensing …*. Retrieved from http://www.isprs.org/proceedings/XXXV/congress/comm3/papers/370.pdf

Lillesand, T. M., & Kiefer, R. W. (1979). Remote sensing and image interpretation. Retrieved from http://ntrs.nasa.gov/search.jsp?R=19810004007

Linder, W. (2009). *Digital photogrammetry*. Retrieved from http://link.springer.com/content/pdf/10.1007/978-3-540-92725-9.pdf

Lohani, B., & Singh, R. (2008). Effect of data density, scan angle, and flying height on the accuracy of building extraction using LiDAR data. *Geocarto International*. Retrieved from http://www.tandfonline.com/doi/abs/10.1080/10106040701207100

Lowe, D. (2004). Distinctive image features from scale-invariant keypoints. *International Journal of Computer Vision*. Retrieved from http://link.springer.com/article/10.1023/B:VISI.0000029664.99615.94

Lucieer, A., Turner, D., King, D. H., & Robinson, S. A. (2014). Using an Unmanned Aerial Vehicle (UAV) to capture micro-topography of Antarctic moss beds. *International Journal*

of Applied Earth Observation and Geoinformation, *27*, 53–62. http://doi.org/10.1016/j.jag.2013.05.011

MacFaden, S. W., O'Neil-Dunne, J. P. M., Royar, A. R., Lu, J. W. T., & Rundle, A. G. (2012). High-resolution tree canopy mapping for New York City using LIDAR and object-based image analysis. *Journal of Applied Remote Sensing*, *6*(1), 063567–1. http://doi.org/10.1117/1.JRS.6.063567

Mancini, F., Dubbini, M., Gattelli, M., Stecchi, F., Fabbri, S., & Gabbianelli, G. (2013). Using Unmanned Aerial Vehicles (UAV) for High-Resolution Reconstruction of Topography: The Structure from Motion Approach on Coastal Environments. *Remote Sensing*, *5*(12), 6880–6898. http://doi.org/10.3390/rs5126880

Mathews, A., & Jensen, J. (2013). Visualizing and Quantifying Vineyard Canopy LAI Using an Unmanned Aerial Vehicle (UAV) Collected High Density Structure from Motion Point Cloud. *Remote Sensing*, *5*(5), 2164–2183. http://doi.org/10.3390/rs5052164

Mayer, S. (2004). *Automatisierte Objekterkennung zur Interpretation hochauflösender Bilddaten in der Erdfernerkundung*.

Moskal, L. M., Styers, D. M., & Halabisky, M. (2011). Monitoring Urban Tree Cover Using Object-Based Image Analysis and Public Domain Remotely Sensed Data. *Remote Sensing*, *3*(12), 2243–2262. http://doi.org/10.3390/rs3102243

Myint, S., & Gober, P. (2011). Per-pixel vs. object-based classification of urban land cover extraction using high spatial resolution imagery. *Remote Sensing of …*. Retrieved from http://www.sciencedirect.com/science/article/pii/S0034425711000034

Nebiker, S., Lack, N., & Deuber, M. (2014). Building Change Detection from Historical Aerial Photographs Using Dense Image Matching and Object-Based Image Analysis. *Remote Sensing*, *6*(9), 8310–8336. http://doi.org/10.3390/rs6098310

PSNERP. (2009). Washington State Data. Retrieved June 11, 2015, from https://wagda.lib.washington.edu/data/geography/wa_state/#PSNERP

Remondino, F. (2011). UAV photogrammetry for mapping and 3d modeling–current status and future perspectives. *… Archives of the …*. Retrieved from http://www.int-arch-photogramm-remote-sens-spatial-inf-sci.net/XXXVIII-1-C22/25/2011/isprsarchives-XXXVIII-1-C22-25-2011.pdf

Reutebuch, S. (2003). Accuracy of a high-resolution lidar terrain model under a conifer forest canopy. *Canadian Journal of …*. Retrieved from http://www.tandfonline.com/doi/abs/10.5589/m03-022

Snavely, N., Seitz, S. M., & Szeliski, R. (2007). Modeling the World from Internet Photo Collections. *International Journal of Computer Vision*, *80*(2), 189–210. http://doi.org/10.1007/s11263-007-0107-3

Sohn, G., & Dowman, I. (2007). Data fusion of high-resolution satellite imagery and LiDAR data for automatic building extraction. *ISPRS Journal of Photogrammetry and Remote …*. Retrieved from http://www.sciencedirect.com/science/article/pii/S0924271607000032

Styers, D. M., Moskal, L. M., Richardson, J. J., & Halabisky, M. A. (2014). Evaluation of the contribution of LiDAR data and postclassification procedures to object-based classification accuracy. *Journal of Applied Remote Sensing*, *8*(1), 083529. http://doi.org/10.1117/1.JRS.8.083529

Suratno, A., Seielstad, C., & Queen, L. (2009). Mapping Tree Species Using LIDAR in Mixed-Coniferous Forests. *Proceedings of Silvilaser 2009*. Retrieved from https://scholar.google.com/scholar?q=Mapping+tree+species+using+LiDAR+in+mixed-coniferous+forests&btnG=&hl=en&as_sdt=0%2C48#0

The Truth about True Orthos | From High Above. (n.d.). Retrieved June 10, 2015, from http://aerometrex.com.au/blog/?p=765

Triggs, B., & McLauchlan, P. (2000). Bundle adjustment—a modern synthesis. *Vision Algorithms: Theory …*. Retrieved from http://link.springer.com/chapter/10.1007/3-540-44480-7_21

Tucker, C. J. (1979). Red and photographic infrared linear combinations for monitoring vegetation. *Remote Sensing of Environment*, *8*(2), 127–150. http://doi.org/10.1016/0034-4257(79)90013-0

Turner, D., Lucieer, A., Malenovský, Z., King, D., & Robinson, S. (2014). Spatial Co-Registration of Ultra-High Resolution Visible, Multispectral and Thermal Images Acquired with a Micro-UAV over Antarctic Moss Beds. *Remote Sensing*, *6*(5), 4003–4024. http://doi.org/10.3390/rs6054003

USGS. (1946). USGS Water Resources NSDI Node. Retrieved June 11, 2015, from http://water.usgs.gov/GIS/metadata/usgswrd/XML/physio.xml

Wang, C., & Glenn, N. (2009). Estimation of fire severity using pre-and post-fire LiDAR data in sagebrush steppe rangelands. *International Journal of Wildland Fire*. Retrieved from http://www.publish.csiro.au/?paper=WF08173

Weng, Q. (2012). Remote sensing of impervious surfaces in the urban areas: Requirements, methods, and trends. *Remote Sensing of Environment*, *117*, 34–49. http://doi.org/10.1016/j.rse.2011.02.030

Williams, G., Thom, R., & Evans, N. (2004). *BAINBRIDGE ISLAND NEARSHORE HABITAT CHARACTERIZATION & ASSESSMENT, MANAGEMENT STRATEGY PRIORITIZATION, AND MONITORING RECOMMENDATIONS*.

Zebedin, L., Klaus, A., Gruber-Geymayer, B., & Karner, K. (2006). Towards 3D map generation from digital aerial images. *ISPRS Journal of Photogrammetry and Remote Sensing*, *60*(6), 413–427. http://doi.org/10.1016/j.isprsjprs.2006.06.005

Zolkos, S., Goetz, S., & Dubayah, R. (2013). A meta-analysis of terrestrial aboveground biomass estimation using lidar remote sensing. *Remote Sensing of Environment*. Retrieved from http://www.sciencedirect.com/science/article/pii/S0034425712004051

Appendix A: List of acronyms

COBI:	City of Bainbridge Island
DHM:	Digital Height Model
DSM:	Digital Surface Model
DTM:	Digital Terrain Model
GCP:	Ground Control Point
GIS:	Geographic Information Systems
GPS:	Global Positioning System
GSD:	Ground Sample Distance
nDSM:	normalized Digital Surface Model
OBIA:	Object Based Image Analysis
NDVI:	Normalized Difference Vegetation Index
NED:	National Elevation Dataset
SfM:	Structure from Motion
SMP:	Shoreline Master Program

Appendix B: List of definitions

datum plane – a plane which serves as a reference or base for the measurement of other quantities

Digital Height Model – DSM of the uppermost surface of a scene

Digital Surface Model – gridded raster image of georeferenced elevation data

Digital Terrain Model – DSM of the bare earth of a scene

ecological function – outputs that benefit organisms with a necessary resource and are the result of interactions of ecological process and structural elements

lidar – light detecting and raging, technology that relies on emission and reception of laser light to measure distance and angle between sensor and subject to produce point clouds

orthophoto – photo that has been geometrically corrected such that the scale is uniform

photogrammetry – the practice of taking spatial measurements from photographs

point cloud – set of data points in some coordinate system

Appendix C: List of files on DVD

bill_point_dhm.tiff
bill_point_dtm.tiff
bill_point_ndsm.tiff
bill_point_ortho.tiff
bill_point_lulc.shp
bill_point_lulc_accuracy.shp
ndsm_validation.csv